

Dynamic Friction and Wear in a Planar-Contact Encapsulated Microball Bearing Using an Integrated Microturbine

Matthew McCarthy, *Member, ASME*, C. Mike Waits, *Member, IEEE*, and Reza Ghodssi, *Member, IEEE*

Abstract—The demonstration and characterization of a novel planar-contact encapsulated microball bearing using a radial inflow microturbine are presented. Stable operation of the air-driven silicon microturbine is shown for over 1 000 000 revolutions at speeds, pressure drops, and flow rates of up to 10 000 r/min, 0.45 lbf/in², and 3.5 slm, respectively. Incorporation of a gas thrust plenum using a novel packaging scheme has enabled comprehensive spin-down friction characterization of the encapsulated microball bearing. An empirical power-law model for dynamic friction has been developed for speeds of 250–5000 r/min and loads of 10–50 mN, corresponding to torques of 0.0625–2.5 $\mu\text{N} \cdot \text{m}$ and friction torque constants of 2.25–5.25 $\times 10^{-4} \mu\text{N} \cdot \text{m}/\text{r}/\text{min}$. The onset and effect of wear and wear debris have been studied, showing negligible wear in the load bearing surfaces for the operating conditions considered. [2008-0109]

Index Terms—Microballs, microelectromechanical systems (MEMS) bearings, microturbines, rolling friction, spin-down.

I. INTRODUCTION

BEARINGS are crucial components in modern machinery, playing a critical role in performance and reliability. They provide a support mechanism for moving parts, greatly reducing friction and wear, and have allowed the realization of a wide variety of technologically advanced rotary machines like motors, generators, pumps, compressors, and turbines. Accordingly, the development of these machines at the micro- and millimeter scales requires a reliable support mechanism that can be easily fabricated and integrated with various components. Microelectromechanical systems (MEMS) fabrication allows for the immediate integration of electric and magnetic elements

for actuation and power generation. Efficient power transmission devices like motors and generators need small gaps manufactured uniformly over relatively large areas, suggesting the need for MEMS fabrication techniques. The achievement of millimeter-scale bearings capable of defining micrometer-scale gaps is a necessity for microactuators and powerMEMS devices. Silicon-based MEMS bearings are desirable over meso-scale bearings made using traditional fabrication processes due to their ability to be scaled down and integrated with electrical and mechanical elements. Micromachines capable of delivering 1–100 mW are envisioned for actuator applications at speeds ranging from 10 to 100 000 r/min. Low-speed rotary positioners for directional sensor systems would only need to overcome bearing friction and operate around 10–100 r/min, while electrically actuated micropumps will require at least 10–100 mW of delivered power at 10 000–100 000 r/min for efficient pumping. High-performance magnetic microgenerators are aimed at producing watt-level power at speeds in excess of 100 000 r/min. In all cases, the power dissipated through bearing friction will ideally count for a small fraction of the overall power, and low-wear operation is a necessity for long life.

While the development of MEMS-fabricated bearings is still in its infancy, several different support mechanisms have been demonstrated for use in micromachines. These include both direct-contact bearings, like flange and center-pin designs [1]–[7], and noncontact bearings, like electrostatic levitation [8], magnetic levitation [9], and gas lubrication [10]–[13]. The first MEMS-fabricated motors used direct-contact bearings and were made from surface micromachined polysilicon. Fan *et al.* [1] and Tai *et al.* [2] demonstrated side-drive variable capacitance micromotors, with diameters of 60–120 μm , using both flange and center-pin bearings. It was concluded that friction played a dominant role in dynamic performance, limiting the devices to speeds of 500 r/min. Mehregany *et al.* [3] have demonstrated harmonic and salient-pole side-drive micromotors supported on direct-contact bearings for speeds of up to 25 000 r/min, with particular emphasis on investigating friction and wear [4], [5]. By monitoring variations in the motor gear ratio, tribological characteristics of the direct-contact bearings were extracted. Significant wear was observed, leading to variations in motor performance over time and limiting overall life. By using these devices and testing procedures, Dhuler *et al.* [6] showed coefficients of friction for the bearing surfaces from 0.38 to 0.55, for a variety of dry gas environments. In addition, Beerschwinger *et al.* [7] have investigated the frictional

Manuscript received April 28, 2008; revised November 21, 2008. First published February 24, 2009; current version published April 1, 2009. This work was supported by the U.S. Army Research Laboratory under Grant CA#W911NF-05-2-0026. Subject Editor L. Lin.

M. McCarthy was with the MEMS Sensors and Actuators Laboratory, Department of Electrical and Computer Engineering, Institute for Systems Research, University of Maryland, College Park, MD 20742 USA. He is now with the Department of Mechanical Engineering, Massachusetts Institute of Technology, Cambridge, MA 02139 USA (e-mail: mattmcc@umd.edu).

C. M. Waits is with the U.S. Army Research Laboratory, Adelphi, MD 20783-1197 USA (e-mail: cwaits@arl.army.mil).

R. Ghodssi is with the MEMS Sensors and Actuators Laboratory, Department of Electrical and Computer Engineering, Institute for Systems Research, University of Maryland, College Park, MD 20742 USA (e-mail: ghodssi@umd.edu).

Color versions of one or more of the figures in this paper are available online at <http://ieeexplore.ieee.org>.

Digital Object Identifier 10.1109/JMEMS.2009.2013407

characteristics of polysilicon microbearings on various substrate materials, finding similar values for coefficient of friction.

The most relevant demonstration of a noncontact MEMS bearing is the gas-lubrication system developed for the *MIT Microengine Project* [10]–[14]. By using hydrostatic thrust and journal bearings, Livermore *et al.* [12] have achieved angular speeds and torques of 55 000 r/min and $3.5 \mu\text{N} \cdot \text{m}$, respectively, in a 4.2-mm-diameter electric induction micromotor. Fr chet te *et al.* [14] have demonstrated 4.2-mm-diameter microturbines supported on fluid film bearings at angular and tip speeds of up to 1.4×10^6 r/min and 300 m/s, respectively, showing the feasibility of these systems for high-power-density turbomachinery applications. Gas-lubricated bearings show a considerable reduction in friction and wear compared to contact-type bearings and have accordingly been used to achieve substantially higher speeds. These systems, however, suffer from fabrication complexity, rotor instability, and the necessity of advanced control schemes. Continued work is required to better understand the stability characteristics of microgas bearings and allow their implementation into practical applications.

With inherent tribological and system-level benefits, microball bearings represent a compromise between the more extensively studied gas-lubricated and contact bearings. Microball bearings provide a simple, stable, and robust support mechanism for PowerMEMS devices. While gas-lubricated systems have superior speed and friction characteristics, microball-bearing-support mechanisms are notably simpler to fabricate and operate. Similarly, microball bearings provide increased tribological performance over sliding contact bearings [15], [16], where friction and wear substantially impact the operation and life of such devices.

In the linear and rotary ball-bearing-supported variable-capacitance micromotors reported by Ghalichechian *et al.* [17]–[19], a silicon slider (or rotor) sits on top of steel microballs housed in rectangular trenches and is actuated via in-plane electrostatic forces. Friction increases with speed until the motors cannot generate enough force/torque to maintain synchronization with the moving element, corresponding to maximum linear and rotary speeds of 7 mm/s and 500 r/min, respectively. Similarly, microturbines supported on encapsulated microball-bearing structures have been demonstrated for speeds up to 37 000 r/min [21]–[23]. These devices, however, are prone to excessive wear, leading to particle contamination and deviations from the as-fabricated geometry. Accordingly, reducing both friction and wear is critical to the realization of ball-bearing-supported high-performance micromachines like rotary MEMS generators, motors, and pumps.

This paper focuses on developing low-friction low-wear bearings through the use of a planar-contact design as well as developing an experimental platform for studying tribological phenomena in current and future devices. Characterizing friction in previous ball-bearing-supported devices was significantly limited by the coupled nature of actuation and normal forces. In the previously published micromotors and turbines [17]–[22], the normal forces were solely dependent on the actuation forces. By using a thrust plenum, these forces have been

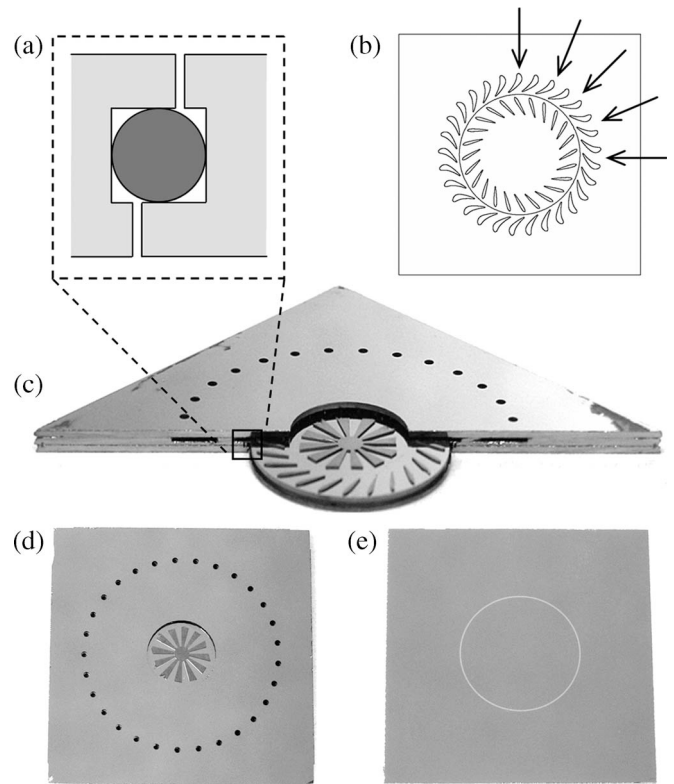


Fig. 1. Microturbine device showing (a) the microball-bearing geometry ($\varnothing = 285 \mu\text{m}$), (b) the blade design and flow direction, and optical photographs of (c) the device cross section with a 10-mm diameter rotor, (d) top side with fluid ports and speed bump structures, and (e) the bottom-side thrust surface. Total device dimensions are $23 \text{ mm} \times 23 \text{ mm} \times 1.5 \text{ mm}$.

decoupled in this paper, allowing for comprehensive spin-down friction testing under a variety of operating conditions relevant to next-generation microball-bearing-supported PowerMEMS devices.

II. MICROTRIBOLOGY DEVICE

A radial in-flow microturbine packaged together with a bottom-side thrust plenum has been developed to investigate the dependence of speed and normal load on dynamic friction and wear in a planar-contact encapsulated microball bearing. Fig. 1(a) and (b) shows illustrations of the novel bearing design, using $285\text{-}\mu\text{m}$ steel microballs, and the turbine actuation mechanism. Fig. 1(c)–(e) shows photographs of the device cross section with a 10-mm-diameter rotor, the topside consisting of a radial array of inlet orifices and a central outlet with rotor speed bumps, and the underside of the encased rotor which acts as a thrust surface. By pressurizing the underside of the packaged turbine rotor, the normal load supported by the microballs can be controlled during spin-down friction testing.

Two noted differences from previous publications are the planar-contact bearing geometry [Fig. 1(a)] and the radial in-flow microturbine design [Fig. 1(b)]. Fig. 2 shows the bearing and turbine designs from the authors' earlier work in encapsulated microball bearings [21], [22]. To minimize friction and wear, the encapsulated microball-bearing fabrication process developed by Waits *et al.* [22] was modified to provide planar [Fig. 1(a)], rather than point [Fig. 2(a)], contact between the

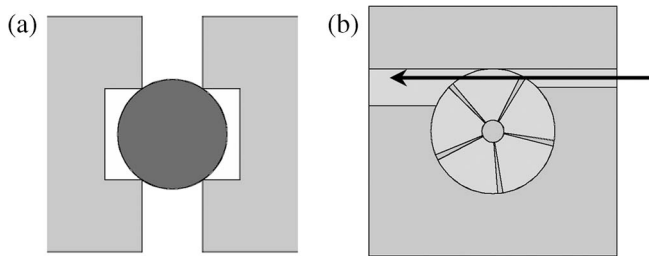


Fig. 2. Conceptual schematics of the previously reported microturbine, showing (a) the point-contact encapsulated microball bearing and (b) the tangential-flow microturbine [21], [22].

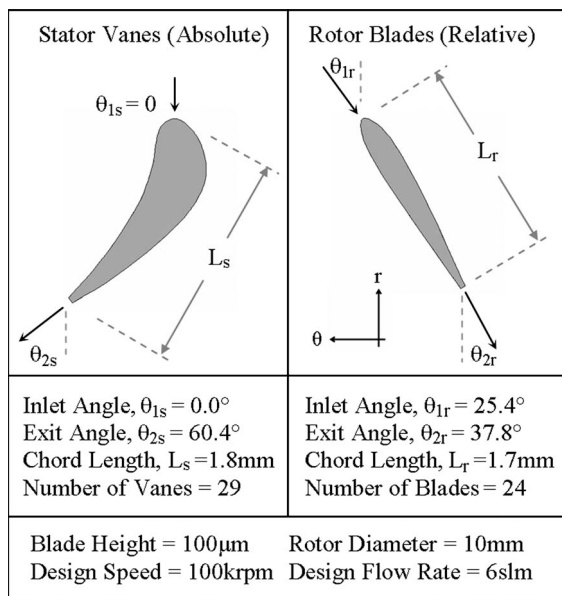


Fig. 3. Microturbine design showing the stator vane and rotor blade geometries in their respective absolute and relative frames of reference.

silicon race and steel microballs. Planar contact between the microballs and the housing reduces stress concentrations and minimizes raceway deformations, as compared to the point-contact design. Similarly, the device presented in this paper uses a radial in-flow microturbine design [Fig. 1(b)] as compared to the previously reported tangential-flow configuration [Fig. 2(b)]. As a result, the turbine is actuated axisymmetrically, evenly distributing the predominantly axial load supported by the microballs over flat contacting surfaces, reducing both friction and wear.

The microturbine was designed, assuming incompressible laminar flow and using a simple velocity-triangle method [24], where the resulting blade geometry and design parameters are shown in Fig. 3. A design speed of 100 000 r/min at a flow rate of 6 slm was chosen, providing 0.5 W of mechanical power. Specifically, the maximum flow velocities and tip speeds were kept well below sonic conditions ($< 50\text{ m/s}$) to meet the assumption of incompressible flow. The microturbine presented here is a convenient actuation mechanism used to characterize the novel microball bearing. Accordingly, no attempts were made to optimize the turbine design, and the only requirement imposed was the ability to span the range of desired rotor speeds.

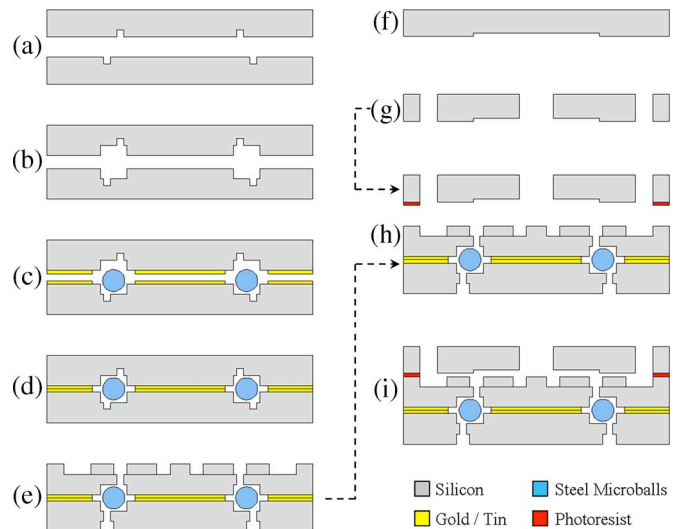


Fig. 4. Microturbine fabrication process flow.

III. FABRICATION

The microturbine fabrication process consists of wafer-level construction of encapsulated rotors followed by die-level temporary bonding of a capping layer to create internal flow paths. First, the microball housing is defined with a nested deep reactive ion etch in a pair of low thickness variation ($< 2\ \mu\text{m}$) silicon wafers [Fig. 4(a) and (b)]. The inner and outer radii of the bearing are 4.910 and 5.205 mm, respectively, creating a 295- μm -wide bearing housing. A 2- μm -thin gold/tin bonding layer is evaporated through a shadow mask, and approximately 90 microballs are placed in the circumferential bearing housing [Fig. 4(c)], filling roughly 85% of the race. This was found to be an acceptable compromise between the minimum number of microballs required to secure the rotor using encapsulation (51% of the race) and the maximum number where ball jamming becomes a predominant failure mode (100% of the race). The microballs (Thompson Precision Balls) are grade ten ball bearings made from 440C stainless steel with a diameter of $285 \pm 0.25\ \mu\text{m}$. The wafers are eutectically bonded [Fig. 4(d)] using the method described in detail by Waits *et al.* [22]. The variation in the deep etch for each side of the ball housings is $\pm 2.5\ \mu\text{m}$ (at a depth of 145.5 μm), and the housing width was measured to vary up to $\pm 2\ \mu\text{m}$. Including the estimated misalignment of the wafers [22] and the bonding layer thickness, the resulting encapsulated microball housing is $295 \pm 5\ \mu\text{m}$ deep \times $295 \pm 7\ \mu\text{m}$ wide, leaving 5–15 μm of vertical and 3–17 μm of lateral play between the balls and the rectangular housing. The wafer stack is diced, and individual die is deep-etched using patterned SiO_2 masks to define the 100- μm -tall turbine blade and speed bump structures as well as to release the rotor [Fig. 4(e)]. The SiO_2 hard masks are defined in each wafer at the very beginning of the fabrication process and have been omitted from Fig. 4.

A silicon capping layer is created with a 25- μm recess to provide 10–20 μm of tip clearance for the spinning rotor blades [Fig. 4(f)], while a through-etch is used to define inlet and outlet ports [Fig. 4(g)]. Finally, the released rotor and capping layer are bonded using a temporary photoresist layer

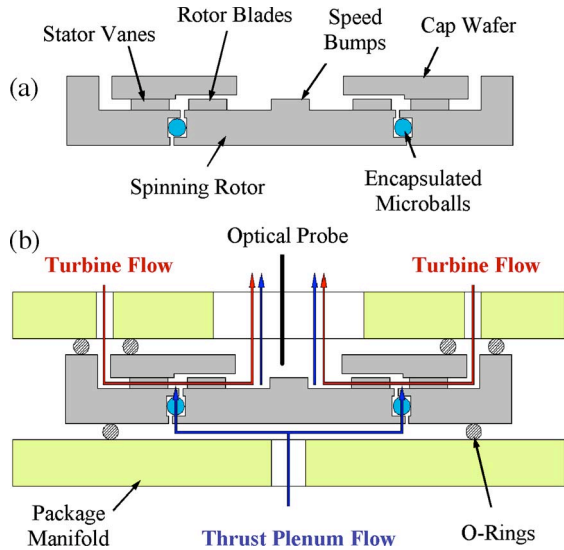


Fig. 5. Schematic showing (a) the microturbine cross section and (b) the experimental operation of the device indicating flow paths for the turbine and thrust plenum.

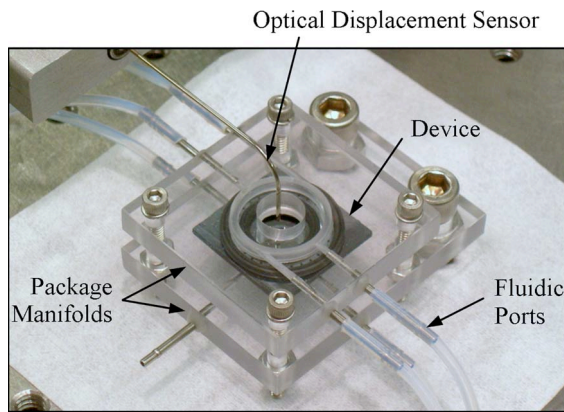


Fig. 6. Photograph of a packaged microturbine being tested.

[Fig. 4(h) and (i)]. As a result, the capping layer can be debonded between tests to examine the turbine and bearing structures. The overall device dimensions are 23 mm \times 23 mm \times 1.5 mm.

IV. EXPERIMENTAL APPARATUS

Figs. 5 and 6 show schematic representations of the device cross section and operation, and a packaged device being tested. Complete characterization of dynamic friction in the planar-contact encapsulated microball bearing requires independent control of bearing speed and thrust load. The decoupling of speed and load during spin-down testing is achieved using a hydrostatic thrust plenum defined by the packaging assembly. The microfabricated turbine is packaged between two plastic manifolds using rubber o-ring seals for fluid delivery as well as compliant support. During operation, the bottom side of the device is pressurized, resulting in a net upward normal force that lifts the rotor into proper contact with the ball bearings. A desired thrust load can be achieved during spin-down testing by supplying thrust plenum flow through a high-sensitivity flow control valve and monitoring the backside

pressure. To actuate the turbine, compressed nitrogen is provided through the topside manifold, while an optical displacement probe tracks the rotation of speed bump structures. The optical displacement sensor (Fig. 6) is located directly above the 12 etched speed bump structures [Fig. 1(d)] at the central exit of the microturbine. As the rotor spins, the sensor outputs a 50% duty-cycle square wave with a frequency 12 times higher than the rotational speed of the turbine. The rotor speed is calculated in real time using LabVIEW via a fast Fourier transform (FFT) of the optical probe signal. Flow rate and pressure drop for both the turbine and thrust plenum are also recorded in LabVIEW. During spin-down testing, the measured thrust plenum flow rate was below the sensitivity of the mass flow meter (< 100 sccm) and more than an order of magnitude less than the turbine flow rates. It is therefore assumed that leakage from the thrust plenum has a negligible effect on the turbine. For spin-down testing, raw data from the optical probe are reduced to obtain angular position versus time; this is due to the insufficient sampling rate of the LabVIEW-FFT scheme. While all tests were performed at ambient temperature and humidity, the bearing and turbine structures were actuated using dry nitrogen, and it is assumed that the results reported here represent bearing friction at 0% relative humidity.

V. RESULTS AND DISCUSSION

A. Microturbine Performance

By using the packaging scheme shown in Figs. 5 and 6, the microturbine has been characterized up to 10 000 r/min and over 1 000 000 revolutions. While this packaging approach allows for independent control of normal and rotational forces during spin-down testing, the two are coupled during turbine actuation. As turbine flow passes over the rotor periphery [Fig. 5(b)], the underside is pressurized, resulting in a net upward normal force, without the addition of thrust plenum flow. Rotational speed, normal force, and turbine flow rate are shown in Fig. 7 as a function of device inlet pressure, in the absence of thrust plenum leakage flow through the bearing.

Fig. 7(a) shows alternate paths for increasing and decreasing actuation at low speeds. This can be attributed to a variety of factors, the simplest of which is the higher static than dynamic friction associated with rolling contact. Starting from rest, the microballs require a larger force (and, therefore, turbine inlet pressure and flow) to initiate rolling, as compared to microballs already in motion. When the turbine is decelerated, it maintains rotation at a driving pressure below the start-up pressure. In addition, variations in the slide-to-roll ratio of the microballs could play a significant role. The slide-to-roll ratio of the microballs is unknown for all ranges of operation, and it is plausible that starting from rest, a larger slide-to-roll ratio leads to higher friction. Another possible contributor is a net radial force on the rotor as a result of slightly asymmetric loading conditions during start-up. Fig. 7(b) shows a linear relationship between inlet pressure and rotor normal force, demonstrating the dependence of normal and rotational forces during actuation. While the microturbines presented here have been successfully actuated in excess of 50 000 r/min, device

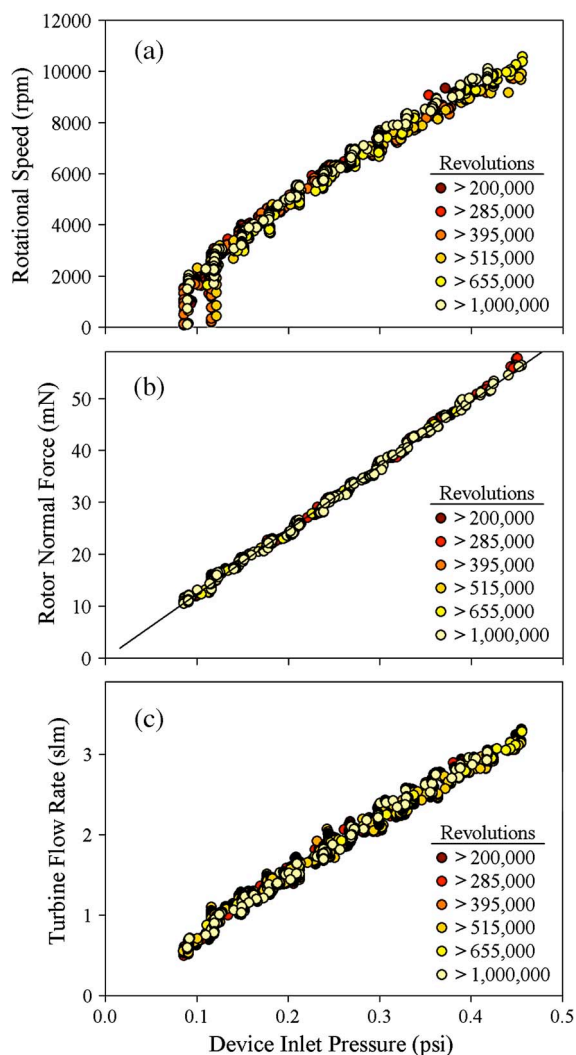


Fig. 7. Turbine operating curves for (a) rotational speed, (b) rotor normal force, and (c) turbine flow rate as a function of inlet pressure, with no thrust plenum flow.

characterization has been restricted to 10 000 r/min. This value was chosen to limit the range of rotor normal forces to those expected in bottom-drive electrostatic micromotors of the same size [18], [19]. In doing so, the friction and wear studies presented here will more closely represent the actual operating conditions, without excessively loading the bearing. When the devices are actuated above 50 000 r/min, the increase in rotor normal force, coupled with the increase in speed, leads to dramatic wear and abrupt failure of the devices.

Fig. 8 shows the results of continuous operation, where the turbines are actuated with 0.25 lbf/in² of driving pressure, resulting in 2 slm of flow and 30 mN of normal force. The rotational speed is seen to decrease after an initial period of consistent operation. This behavior has been attributed to the buildup wear debris, slowing the rotor due to increased friction associated with particle contamination. Accordingly, the device was periodically cleaned in an acetone bath with ultrasonic agitation to remove wear particles. After ultrasonic cleaning, the turbine performance returns to the expected behavior, showing longer operation with increased revolutions; this implies a decreasing wear rate over time. Each data set

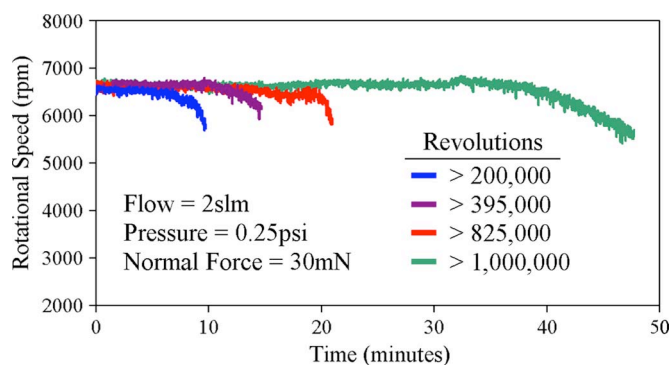


Fig. 8. Effect of wear debris on performance after prolonged operation. After each data set, the device is cleaned and returns to the expected behavior.

of the characterization curves in Fig. 7(a)–(c) was collected after ultrasonic cleaning. This suggests that while wear debris limits the device endurance (the duration of time before the onset of contamination, as shown in Fig. 8), wear itself (the geometric deviation from the as-fabricated state) has little effect on performance in the clean state [Fig. 7(a)–(c)]. This is a counterintuitive result and would suggest that the wear particles contaminating the microball housing are not being generated from the load-bearing contact interfaces. This hypothesis will be discussed further in a subsequent section.

B. Spin-Down Friction Testing

Comprehensive characterization of dynamic bearing friction is achieved through spin-down testing using the backside thrust plenum [Fig. 2(b)] to achieve a desired rotor normal force. The spin-down response of the microturbine can be separated into three distinct stages, as shown in Fig. 9. Initially, the turbine is spinning at a constant speed ($\sim 10\,000$ r/min) corresponding to a linear increase in angular position and an elevated constant thrust force (stage *a*). Then, the turbine flow is shut off, and the thrust force decreases dramatically as the rotor begins to slow down (stage *b*). Finally, stage *c* corresponds to the period after the thrust load equilibrates to within 10% of the preset desired value. Spin-down data are acquired during stage *c*. An optical probe measures the angular position θ as the rotor decelerates under a prescribed constant normal force provided by the thrust plenum. The normal force is calculated as the product of the rotor area and the measured backside pressure. Spin-down friction testing is conducted immediately following ultrasonic cleaning of the device. It requires 2–3 min of turbine operation and less than 20 000 revolutions for each interval considered. It is therefore assumed that the effects of wear debris are negligible over these durations as would be suggested by the results shown in Fig. 8.

In addition, it is assumed that fluidic losses in the microturbine are small compared to bearing friction. Reynolds numbers based on blade height and tip speed at the rotor periphery vary from 1 to 25 during spin-down testing. At such low Reynolds numbers, skin friction effects can be assumed dominant over pressure drag [25]. Under the assumption of fully developed coquette flow through the turbine blade tip clearances and on the underside of the rotor, it is estimated that viscous friction in

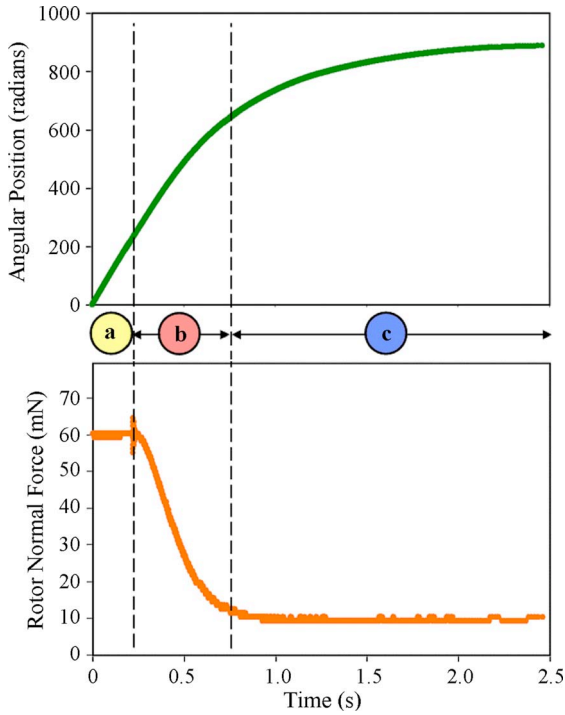


Fig. 9. Spin-down data acquisition procedure. (a) The turbine is spun at a constant speed of 10 000 r/min. (b) The turbine flow is shut off, and the speed and normal force decrease. (c) The normal force equilibrates to the preset value; spin-down data are acquired during this stage as the rotor decelerates under a specified constant normal force.

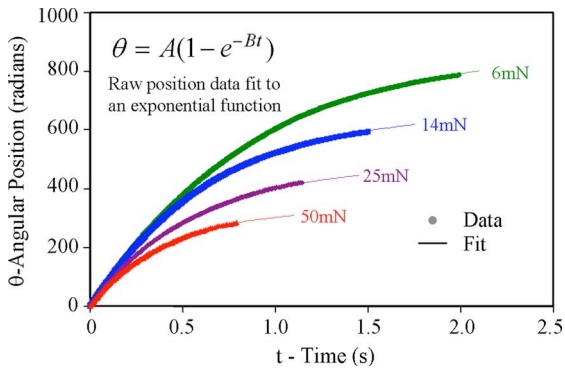


Fig. 10. Spin-down trajectory data for several normal loads fit to an exponential function with constants A and B , resulting in a linear relationship between deceleration and speed.

these components makes up less than 5% of the total measured friction torque. This is due to relatively large rotor blade tip clearance gaps ($> 10 \mu\text{m}$), small tip clearance areas, and the large distance between the rotor underside and the package (1.5 mm). Viscous effects occurring within the actual microball bearing housing are considered small but inherent components of bearing friction and should be included in the characterization. It is therefore assumed that fluidic effects comprise a small percentage of the total resistance and the friction measurements reported here are representative of the bearing itself.

To characterize the effects of speed and load on dynamic bearing friction, the testing procedure is repeated for several normal loads. Fig. 10 shows spin-down data acquired at several thrust forces, showing faster spin-down at higher loads, as

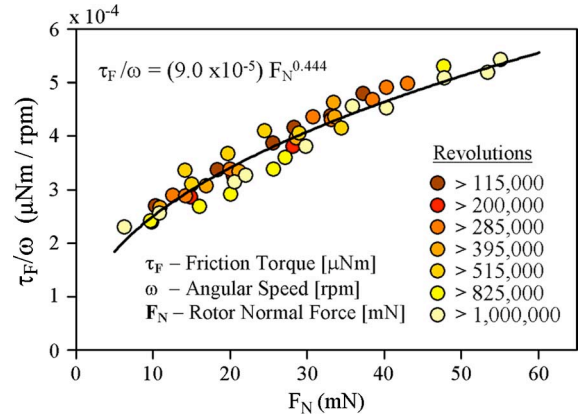


Fig. 11. Friction torque constant as a function of rotor normal force at various intervals, showing good agreement with a power-law relation up to 1 000 000 revolutions.

would be expected. These position versus time data sets fit well to an exponential function of the form

$$\theta = A(1 - e^{-Bt}) \tag{1}$$

(with coefficients A and B). The result is a linear relationship between angular acceleration ($\ddot{\theta}$) and angular velocity ($\dot{\theta}$)

$$\ddot{\theta} = -B\dot{\theta} \tag{2}$$

and, therefore, a linear relationship between friction torque, calculated as the product of the angular acceleration and rotor mass moment of inertia ($\tau_F = I\ddot{\theta}$), and bearing speed ($\omega = \dot{\theta}$). Accordingly, each spin-down at a constant normal force (F_N) corresponds to a single ratio of friction torque to rotational speed

$$\frac{\tau_F}{\omega} = |I \cdot B| = f(F_N) \tag{3}$$

(referred to here as the friction torque constant) where I is the rotor mass moment of inertia and B is the coefficient determined from numerical fitting.

This testing and data reduction scheme is repeated sequentially at various intervals up to 1 000 000 revolutions for normal loads from 10 to 50 mN. These loads correspond to the range of expected values in next-generation electrostatic and magnetic micromotors and microgenerators supported on microball bearings [19]. The dependence of friction torque constant (τ_F/ω) on the normal load (F_N) is shown in Fig. 11 for intervals up to 1 000 000 revolutions. Dynamic friction torque has been characterized for speeds and loads of 250–5000 r/min and 10–50 mN, respectively, corresponding to 0.0625–2.5 $\mu\text{N} \cdot \text{m}$ of friction torque. By using these results, the microball bearings exhibit velocity and load-dependent coefficients of dynamic friction (defined as the ratio of tangential friction force to normal force) varying from 0.0005 (at 250 r/min and 50 mN) to 0.025 (at 5000 r/min and 10 mN). Over the operating ranges considered here, the dynamic friction torque was found to fit well to an empirically derived power-law model using two modeling constants (C and D). A linear relationship between friction torque and speed has been observed, while friction increases as the normal force to the power of $D = 0.444$. The

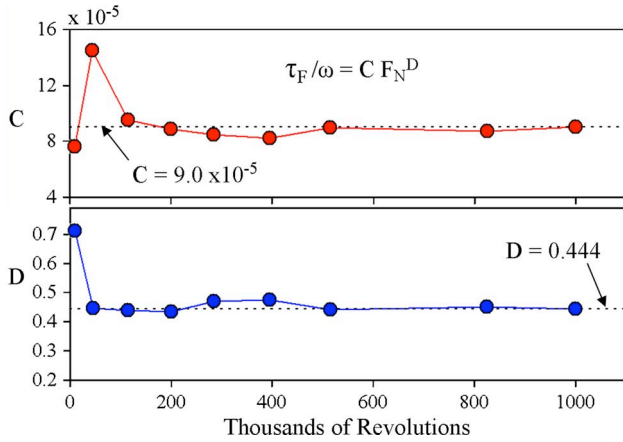


Fig. 12. Empirical modeling constants from spin-down friction tests, equilibrating after an initial period of wear.

constant of proportionality in the empirical power-law model is $C = 9 \times 10^{-5} \mu\text{N} \cdot \text{m}/\text{mN}^{0.444} \cdot \text{r}/\text{min}$, such that

$$\tau_F = (9.0 \times 10^{-5}) F_N^{0.444} \omega. \quad (4)$$

Fig. 12 shows the evolution of these modeling constants at every interval. After an initial period of “run-in”, consistent results from 100 000 to 1 000 000 revolutions are observed corresponding to the empirical friction model of (4).

These results show that 0.025 mW of power is dissipated at 1000 r/min under a normal load of 10 mN. If it is assumed that the model given by (4) holds true for higher speeds, then 2.5 and 250 mW will be dissipated at speeds of 10 000 and 100 000 r/min, respectively. This demonstrates the amount of power needed to be transferred at various speed ranges for such bearings to be efficient support mechanisms. Electrically actuated devices (motors, pumps, etc.) designed to operate around 10 000 r/min will require up to several milliwatts of power for efficient operation, and turbine-driven devices (microturbogenerators) will require watt-level power. While these ranges are acceptable for next-generation MEMS devices, the developed platform will be used to investigate and reduce bearing friction by minimizing normal load and depositing tribological hard coatings.

C. Comparison to Conventional Ball Bearings

Bearings fabricated using macroscale techniques have been optimized for decades and use a variety of advanced materials, components, geometries, and lubricants. While conventional ball bearings have several key differences to those presented here, they can be compared to MEMS-fabricated bearings on the basis of size, speed, and friction. Speed limitations are dependent on many factors, such as the bearing materials, raceway design, cage material, lubrication type, tolerance, and loading conditions. In most ball-bearing designs at the scale developed in this paper, the bearing contains a ball cage to isolate the balls from contacting each other. In addition to the cage, bearings of this size usually use oil or grease lubrication. A well-established means of defining bearing speed is the DN value, the product of bearing diameter (in millimeters) and the rotational speed (in revolutions per minute). For 10-mm

outer-diameter deep-groove and angular-contact bearings, typical manufacturer speed limitations are from 25 000 r/min ($DN = 250\,000$) to 60 000 r/min ($DN = 600\,000$) and increase with a reduction in size. These values are representative of average bearing performance, and high-speed bearings ($DN > 1\,000\,000$) are not uncommon.

In this paper, the raceway is completely filled with the balls and no cage is used; this is due to limitations in microfabrication capabilities. The inclusion of liquid lubricants into microbearings is likely problematic due to high static friction, large evaporation rates, and the complexity of maintaining constant lubrication over long operating times. In addition, the ratio of ball diameter to rotor diameter for the microball bearings (0.0285) is notably lower than those in macrofabricated thrust-loaded ball bearings where values around 0.1–0.2 are typical [26]. Nevertheless, the microball bearings have been demonstrated at speeds and rolling resistances comparable to the ranges seen in typical macrofabricated bearing mechanisms of the same size. The microball bearings have been characterized up to 10 000 r/min ($DN = 100\,000$) with peak measured speeds of 50 000 r/min ($DN = 500\,000$). The coefficient of friction (defined as the ratio of tangential friction force to normal force) has been measured to be as low as 0.0005 for low-speed high-load operation, while typical values in the range of 0.0001–0.0005 are reported for conventional bearings [26]. Long-term operation of microball bearings has yet to be demonstrated, and this will most likely require technological advancements similar to those used in conventional bearings, namely, tailoring the geometry and materials of the contact interfaces. While it is unlikely that MEMS-fabricated bearings will surpass the performance of macrofabricated bearings, these results show a promise for their development as stable and reliable support mechanisms capable of being integrated with complex microsystems.

D. Comparison to MEMS Bearings

The microball-bearing performance can be compared to gas-lubricated MEMS bearings via the viscous torque constant, a direct analogy to the friction torque constant described here (τ_F/ω), where viscous drag resists rotation rather than rolling friction. The electric induction micromotor supported on fluid film bearings developed by Livermore *et al.* [12] operated at a maximum tip speed of 11.5 m/s, and a viscous torque constant of $(5.9 \pm 0.96) \times 10^{-5} \mu\text{N} \cdot \text{m}/\text{r}/\text{min}$ was measured using experimental spin-down testing. Fréchette *et al.* [13], [14] have reported viscous torque constants as low as $2 \times 10^{-5} \mu\text{N} \cdot \text{m}/\text{r}/\text{min}$ in microfabricated induction motors and turbomachinery through spin-down characterization and theoretical calculations. This paper shows friction torque constants as low as $(22.5 \pm 5) \times 10^{-5} \mu\text{N} \cdot \text{m}/\text{r}/\text{min}$, for a normal force of 10 mN, with a maximum tip speed of 5.2 m/s. It should be noted that the gas-lubricated viscous torque constant constitutes the total viscous drag, including effects from the journal and thrust bearings as well as the electrostatic motor and other surfaces in close proximity with the rotor. Accordingly, an electrostatic microball-bearing-supported device would have additional components of drag not considered in this paper, such as those

acting over small gaps associated with electrostatic actuation or generation.

While the achievement of friction characteristics comparable to those demonstrated in fluid film bearings may not be possible, this paper demonstrates a notable decrease in fabrication and operation complexities as well as an increase in robustness as compared to air bearings. The microturbines reported here have been fabricated using relatively simple processes with nearly 100% yield and are inherently immune to the dramatic and catastrophic failures reported in gas-lubricated systems. While contamination due to excessive wear has been observed, the devices do not suffer from stability issues associated with natural frequency as in air bearings. Similarly, the bearing considered here shows a decrease in coefficient of dynamic friction of several orders of magnitude as compared to direct-contact sliding bearings operated at comparable speeds [6]. Optimized microball bearings using tribological coatings and axially balanced rotors are envisioned for maximum operating speeds of 100 000–200 000 r/min, tips speeds of less than 100 m/s, and friction torques on the order of 1–10 $\mu\text{N}\cdot\text{m}$. This is a notably lower speed than that achieved using the fluid film bearings developed by Fr chet te *et al.*, demonstrating 1 400 000 r/min and tip speeds of 300 m/s [14].

E. Comparison to Analytic Predictions

An empirical model for bearing friction has been developed for a range of speeds and loads by directly measuring rotor deceleration and, therefore, friction torque. An alternative indirect method of friction modeling could be derived analytically from the turbine torque, although it suffers from fundamental uncertainties requiring complex and impractical computational modeling. The comparison of these two techniques will be presented in this section.

Neglecting the effects of viscous losses, the torque applied to the rotor from the working fluid is balanced by friction generated in the microball bearing. Accordingly, the friction torque can be evaluated using theoretical means. Applying the conservation of angular momentum, the torque is equal to the time rate of change of angular momentum in a streamtube flowing through the device [24], expressed analytically as

$$\tau_F = \dot{m}(r_L V_L - r_T V_T) \tag{5}$$

where \dot{m} is the mass flow rate, r is the radial location, and V is the tangential velocity of the fluid in the absolute frame, where the subscripts L and T represent the rotor blade leading and trailing edges, respectively. Defining the absolute tangential flow velocities (V_L and V_T) in terms of mass flow rate, rotor speed, and blade geometry, (5) can be reduced to

$$\tau_F = \dot{m} \left[\frac{\dot{m}}{2\pi\rho h} (\tan(\theta_{2s} + \delta\theta_{2s}) + \tan(\theta_{2r} + \delta\theta_{2r})) - r_T^2 \omega \right] \tag{6}$$

where ρ is the fluid density, h is the blade height, θ_{2s} and θ_{2r} are the stator vane and rotor blade exit angles (using the convention defined in Fig. 3), and $\delta\theta_{2s}$ and $\delta\theta_{2r}$ are the deviations of the actual flow velocities from the ideal blade angles.

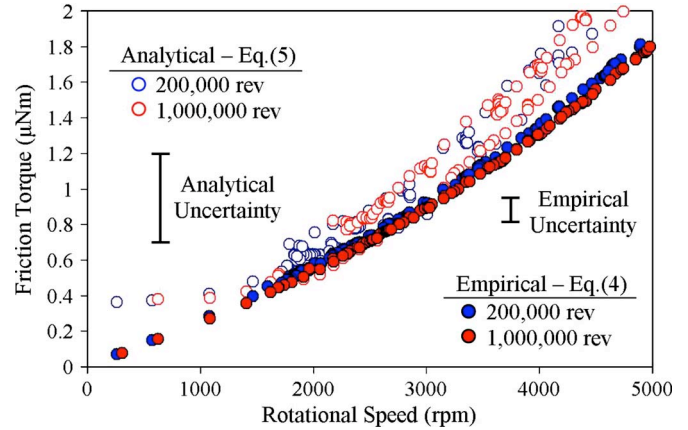


Fig. 13. Comparison of friction torque calculated using experimental data with both the analytical and empirical models of (5) and (4), respectively.

In macroscale turbomachinery, the exit flow deviations ($\delta\theta_{2s}$ and $\delta\theta_{2r}$) depend on blade geometry, inlet incidence angle, and flow Mach number. In addition, Lee *et al.* [27], [28] have shown a strong dependence between flow deviation and Reynolds number (Re) in microturbomachinery, for $100 < Re < 1000$, where Re is defined using the chord length and inlet conditions. By using computational fluid dynamics (CFD), Lee has shown that for a rotor blade cascade with a solidity and chamber comparable to the microturbine in this paper, the exit flow angle varies nonlinearly up to $\pm 10\%$ of the designed blade angle, over the range of Re considered here ($100 < Re < 1000$). The power delivered to the turbine will be altered by flow deviations as well as several other factors creating variations during actual operation. As the boundary layer grows, the effective blade height will be reduced by flow blockage. In addition, tip clearance flow between the rotor blades and the capping wafer will reduce the total effective mass flow rate and, therefore, the torque applied to the rotor. These phenomena have complex relationships with various flow parameters and therefore change with operating conditions. Typically, CFD is necessary to accurately model these effects.

In the absence of comprehensive CFD modeling, the theoretical approximation for friction torque in (6) cannot be confidently implemented to characterize the microball bearings, due to variations arising in the actual flow. For comparison purposes, friction torque has been calculated using both the developed empirical model [see (4)] and the analytical model [see (6)] and is shown in Fig. 13. Experimental measurements of rotational speed, mass flow rate, and normal force were used to calculate torque, while the flow angles were assumed to be identical to the as-fabricated blade angles (θ_{2s} and θ_{2r} in Fig. 3). In these calculations, the analytical uncertainty is based on $\pm 10\%$ exit flow deviations from the defined blade angles, and the empirical uncertainty is based on the error in the power-law curve fitting shown in Fig. 11. This analysis does not take into consideration the effects of blockage or tip clearance flow. Fig. 13 shows the friction torque calculated after 200 000 and 1 000 000 revolutions with negligible variations between the two. It can be seen that the analytically calculated torque has a larger scatter as compared to the empirical. This is a product of fluctuations in the mass flow measurements used

to calculate the analytical results; the empirically calculated values are based on speed and pressure measurements alone which have much smaller fluctuations. The variations between the analytical and empirical results are attributed to an inability to predict, among other things, exit flow deviations, blockage, and tip clearance flow. These results show general agreement between the two approaches, validating the empirical modeling approach based on spin-down testing. They simultaneously address the large uncertainty in an analytically derived friction measurement technique. The larger predicted values of torque in Fig. 13 are consistent with the effects of tip clearance and flow deviation, where less mass flow rate is being turned by the rotor blades and producing torque. This variability in the analytic model highlights the necessity of the empirically derived model developed and the spin-down approach used in this paper.

F. Wear

The effects of wear are equally as important as friction to the realization of microball-bearing-support mechanisms for rotary MEMS devices. Accordingly, the microturbine was disassembled to examine the state of wear on the microballs and within the bearing housing upon completion of the previously described experiments. Wear on the balls themselves was virtually unnoticeable when examined using SEM imaging and appeared only as a smoothing of the as-manufactured stainless steel balls. This is likely due to the relatively large total surface area of the microballs as compared to the raceways. As the rotor spins, the balls are free to rotate in all directions, and only a small fraction of the available surface area is in contact at any given instant. The silicon housing, however, experiences repeated loading and unloading over a much smaller and constant area.

The planar-contact raceway design, shown schematically in Fig. 1, has four points of possible contact: first and foremost, the race surfaces on both the rotor and stator, which support the axial thrust load, and second, the sidewalls of the bearing housing, which support radial loads. Fig. 14 shows a SEM image of the rotor periphery where the turbine rotor blades can be seen, along with the identification of these two critical locations exhibiting wear. Due to the symmetric nature of the encapsulated bearing housing, a wafer bond interface exists directly at the point of contact between the microballs and the housing sidewall. Fig. 15 shows the unworn and worn race surfaces and bond interfaces, where the worn device was actuated for over 1 000 000 revolutions at an average speed and normal force of 6000 r/min and 30 mN, respectively.

Fig. 15(a) and (b) shows the race surfaces (the primary load-bearing surfaces used to support the normal thrust force) for unworn and worn devices. As can be seen, an obvious fabrication defect exists on the edge of this surface. This defect is a product of the nested etches used to define the housing in Fig. 4(a) and (b). The housing is designed such that the microball contacts are far enough from the edge not to interfere with this defect. A wear track less than 15 μm wide can be seen in Fig. 15(b). While the wear track is visible in SEM imaging, the depth was too small to measure using optical profilometry and, therefore, indistinguishable from the roughness, measured

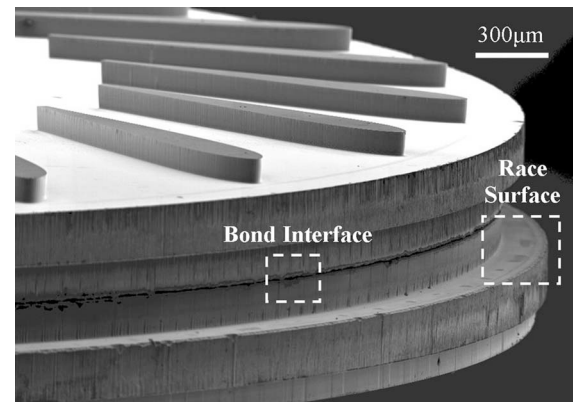


Fig. 14. SEM image of the rotor periphery identifying the race surface and the sidewall bond interface locations exhibiting wear.

to be less than 100 nm. This is a marked improvement from the earlier point-contact designs [21], [22], where over 12 μm of wear was seen for similar loading conditions. The resistance to wear is critical in the realization of rotary micromotors and microgenerators where a consistent and known gap between the rotor and electrical/magnetic stator elements is crucial.

Fig. 15(c) and (d) shows the bond interface on the bearing housing sidewall for unworn and worn devices. While the design of this device addressed the reduction of wear by using a planar-contact geometry, insufficient consideration was given to wear on the housing sidewall. The wafer-level eutectic bonding procedure [Fig. 4(d)] used to encapsulate the microballs led to a poorly placed bond interface. While radial loads are significantly lower than axial loads, the nature of the free edges at the bond interface creates stress concentrations, resulting in excessive wear and particle generation. Fig. 15(c) shows the unworn bond interface, and Fig. 15(d) shows the bond interface after 1 000 000 revolutions.

The SEM images in Fig. 15 shed light on the counterintuitive results discussed in the *Microturbine Performance* section, where wear particles slowed the turbine but had virtually no effect on performance after being cleaned. This suggests that rolling friction at the race surfaces is the predominant cause of friction torque and therefore dictates turbine performance. These surfaces showed negligible wear, and therefore, negligible change in performance was seen when operated in the clean state. Chipping and wearing at the sidewall bond interface generates the wear debris, slowing the turbine after continuous operation, but has an insignificant effect on friction (and therefore performance) in the clean state, because it supports only minor radial loads.

Based on the results presented here, a critical modification to the bearing structure is being implemented in future designs. By simply adjusting the depths of the etches used to create the bearing housing, the bond interface can be offset from the contacting microballs. This will greatly improve the endurance and performance of the planar-contact encapsulated bearing.

VI. CONCLUSION

Stable operation of a silicon microturbine supported on a novel planar-contact encapsulated microball bearing has been

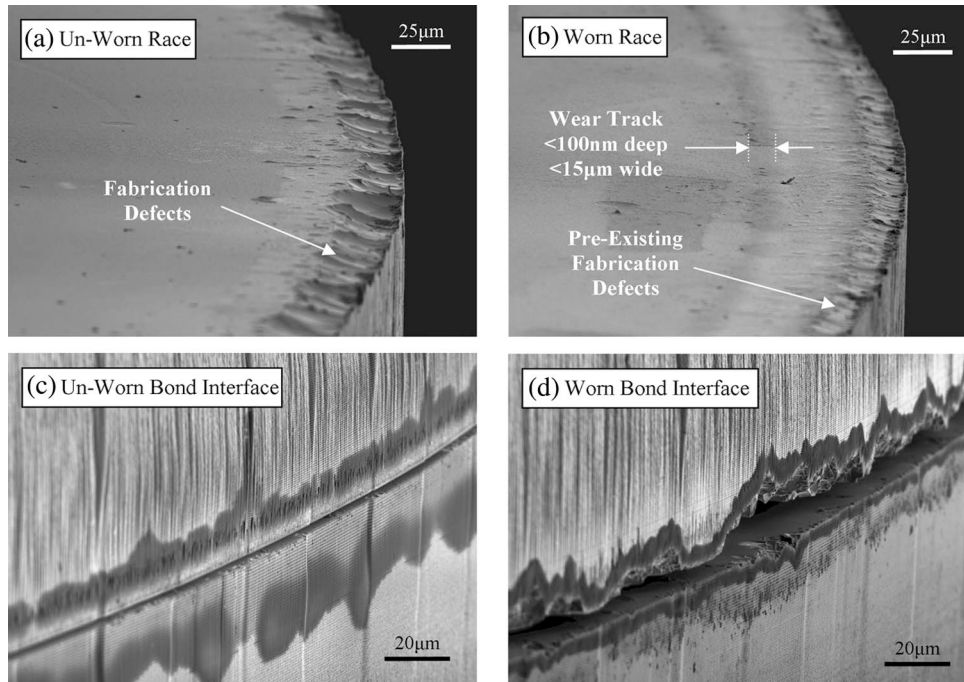


Fig. 15. Comparison of the bearing race surfaces and bond interfaces of an unworn device and a device after 1 000 000 revolutions at an average speed and normal force of 6000 r/min and 30 mN, respectively. (a) Unworn race. (b) Worn race. (c) Unworn bond interface. (d) Worn bond interface.

demonstrated for over 1 000 000 revolutions at speeds, pressure drops, and flow rates of up to 10 000 r/min, 0.45 lbf/in², and 3.5 slm, respectively. The devices and testing apparatus presented here have enabled the first characterization and empirical modeling of dynamic friction in microball bearings over operating conditions relevant to the development of a wide range of rotary PowerMEMS devices, corresponding to torques of 0.0625–2.5 $\mu\text{N} \cdot \text{m}$, friction coefficients of 0.0005–0.025, and friction torque constants of $2.25\text{--}5.25 \times 10^{-4} \mu\text{N} \cdot \text{m/r/min}$. This is the first demonstration of such a system, independently investigating the effects of speed and load, through the use of a hydrostatic thrust plenum. This apparatus has provided quantitative and qualitative information on the nature and prominence of friction and wear in microball bearings, leading to relevant geometric design modifications. In addition, the device and testing platform presented in this paper will be used to study the effects of humidity and hard coatings on friction and wear in microball bearings. The technologies presented here will act as the basis for developing robust drive and support mechanisms for rotary microgenerators, motors, electric pumps, and turbopumps.

ACKNOWLEDGMENT

The authors would like to thank N. Siwak for the SEM images contained in this paper.

REFERENCES

- [1] L.-S. Fan, Y.-C. Tai, and R. S. Muller, "IC-processed electrostatic micro-motors," in *IEDM Tech. Dig.*, San Francisco, CA, 1988, pp. 666–669.
- [2] Y. C. Tai, L. S. Fan, and R. S. Muller, "IC processed micro-motors: Design, technology, and testing," in *Proc. IEEE Microelectromech. Syst.*, Salt Lake City, UT, 1989, pp. 1–6.
- [3] M. Mehregany, S. F. Bart, L. S. Tavrow, J. H. Lang, and S. D. Senturia, "Principles in design and microfabrication of variable-capacitance side-drive motors," *J. Vac. Sci. Technol. A, Vac. Surf. Films*, vol. 8, no. 4, pp. 3614–3624, Jul. 1990.
- [4] M. Mehregany, S. D. Senturia, and J. H. Lang, "Friction and wear in microfabricated harmonic side-drive motors," in *Proc. Solid-State Sens., Actuators Microsyst. Workshop*, Hilton Head Island, SC, 1990, pp. 17–22.
- [5] M. Mehregany, S. Senturia, and J. Lang, "Measurement of wear in polysilicon micromotors," *IEEE Trans. Electron Devices*, vol. 39, no. 5, pp. 1136–1143, May 1992.
- [6] V. R. Dhuler, M. Mehregany, and S. M. Phillips, "A comparative study of bearing designs and operational environments for harmonic side-drive micromotors," *IEEE Trans. Electron Devices*, vol. 40, no. 11, pp. 1985–1989, Nov. 1993.
- [7] U. Beerschwinger, R. L. Reuben, and S. J. Yang, "Frictional study of micromotor bearings," *Sens. Actuators A, Phys.*, vol. 63, no. 3, pp. 229–241, Dec. 1997.
- [8] S. Kumar, D. Cho, and W. Carr, "A proposal for electrically levitating micromotors," *Sens. Actuators A, Phys.*, vol. 24, no. 2, pp. 141–149, Jul. 1990.
- [9] K. Komori and T. Yamane, "Magnetically levitated micro PM motors by two types of active magnetic bearings," *IEEE/ASME Trans. Mechatronics*, vol. 6, no. 1, pp. 43–49, Mar. 2001.
- [10] A. H. Epstein, S. D. Senturia, O. Al-Midani, G. Anathasuresh, A. Ayon, K. Breuer, K.-S. Chen, F. F. Ehrlich, E. Esteve, and L. Frechette, "Micro-heat engine, gas turbine, and rocket engines—The MIT microengine project," presented at the 28th AIAA Fluid Dynamics Conf., Snowmass Village, CO, Jun. 1997.
- [11] F. F. Ehrlich and S. A. Jacobson, "Development of high-speed gas bearings for high-power density microdevices," *ASME J. Eng. Gas Turbines Power*, vol. 125, no. 1, pp. 141–148, Jan. 2003.
- [12] C. Livermore, A. Forte, T. Lyszczara, S. D. Umans, and J. H. Lang, "A high-power MEMS electric induction motor," *J. Microelectromech. Syst.*, vol. 13, no. 3, pp. 465–471, Jun. 2004.
- [13] L. G. Fréchet, S. F. Nagle, R. Ghodssi, S. D. Umans, M. A. Schmidt, and J. H. Lang, "An electrostatic induction micromotor supported on gas-lubricated bearings," in *Proc. IEEE Microelectromech. Syst.*, Interlaken, Switzerland, Jan. 21–25, 2001, pp. 290–293.
- [14] L. G. Fréchet, S. A. Jacobson, K. S. Breuer, F. F. Ehrlich, R. Ghodssi, R. Khanna, C. W. Wong, X. Zhang, M. A. Schmidt, and A. Epstein, "High-speed microfabricated silicon turbomachinery and fluid film bearings," *J. Microelectromech. Syst.*, vol. 14, no. 1, pp. 141–152, Feb. 2005.
- [15] T.-W. Lin, A. Modafe, B. Shapiro, and R. Ghodssi, "Characterization of dynamic friction in MEMS-based microball bearings," *IEEE Trans. Instrum. Meas.*, vol. 53, no. 3, pp. 839–846, Jun. 2004.

- [16] X. Tan, A. Modafe, and R. Ghodssi, "Measurement and modeling of dynamic rolling friction in linear microball bearings," *Trans. ASME, J. Dyn. Syst. Meas. Control*, vol. 128, no. 4, pp. 891–898, Dec. 2006.
- [17] N. Ghalichechian, A. Modafe, J. H. Lang, and R. Ghodssi, "Dynamic characterization of a linear electrostatic micromotor supported on microball bearings," *Sens. Actuators A, Phys.*, vol. 136, no. 2, pp. 416–503, May 2007.
- [18] N. Ghalichechian, A. Modafe, M. Beyaz, and R. Ghodssi, "Design, fabrication, and characterization of a rotary micromotor supported on microball bearings," *J. Microelectromech. Syst.*, vol. 17, no. 3, pp. 632–642, Jun. 2008.
- [19] N. Ghalichechian, "Design, fabrication, and characterization of rotary variable-capacitance micromotor supported on microball bearings," Ph.D. dissertation, Univ. Maryland, College Park, MD, 2007.
- [20] N. Ghalichechian, M. McCarthy, M. Beyaz, and R. Ghodssi, "Measurement and modeling of friction in linear and rotary micromotors supported on microball bearings," in *Proc. IEEE Microelectromech. Syst.*, Tucson, AZ, Jan. 13–17, 2008, pp. 507–510.
- [21] C. M. Waits, N. Jankowski, B. Geil, and R. Ghodssi, "MEMS rotary actuator using an integrated ball bearing and air turbine," in *Proc. Int. Conf. Solid-State Sens. Microsyst.*, Lyon, France, Jun. 10–14, 2007, pp. 1131–1134.
- [22] C. M. Waits, B. Geil, and R. Ghodssi, "Encapsulated ball bearings for rotary micromachines," *J. Micromech. Microeng.*, vol. 17, no. 9, pp. S224–S229, Sep. 2007.
- [23] M. McCarthy, C. M. Waits, and R. Ghodssi, "Development of a hybrid gas/ball bearing support mechanism for microturbomachinery," in *Proc. Int. Workshop Micro Nanotechnol. Power Gen. Energy Convers.*, Freiburg, Germany, Nov. 28–29, 2007, pp. 241–244.
- [24] R. I. Lewis, *Turbomachinery Performance Analysis*. Hoboken, NJ: Wiley, 1996.
- [25] R. W. Fox and A. T. McDonald, *Introduction to Fluid Mechanics*. Hoboken, NJ: Wiley, 1998.
- [26] T. A. Harris and M. N. Kotzalas, *Rolling Bearing Analysis: Essential Concept of Bearing Technology*. Boca Raton, FL: CRC Press, 2006.
- [27] C. Lee, S. Arslan, and L. G. Fr chet, "Design principles and aerodynamics of low Reynolds multi-stage microturbomachinery," in *Proc. ASME Int. Mech. Eng. Congr. Expo.*, Anaheim, CA, Nov. 13–19, 2004.
- [28] C. Lee, "Development of a microfabricated turbopump for a rankine vapor power cycle," Ph.D. dissertation, Columbia Univ., New York, NY, 2006.



C. Mike Waits (S'01–M'08) received the B.S. degree in physics from Salisbury University, Salisbury, MD, in 2000, and the M.S. and Ph.D. degrees in electrical engineering from the University of Maryland, College Park, in 2003 and 2008, respectively.

He joined the Sensors and Electron Devices Directorate, U.S. Army Research Laboratory, Adelphi, MD, as an Electronics Engineer in 2004. His main research interests include MEMS components and systems focused on power and energy generation and conversion (power MEMS), MEMS tribology and bearing mechanisms, and new microfabrication techniques.

Dr. Waits was the recipient of the Physics Excellence Award from Salisbury University in 2000, the Graduate Assistance in Areas of National Need (GAAN) Fellowship in 2001–2003, and Department of the Army Research and Development Achievement Award for Technical Excellence in 2007.



Matthew McCarthy received the B.S. degree in aerospace engineering from Syracuse University, Syracuse, NY, in 2002 and the M.S. and Ph.D. degrees in mechanical engineering from Columbia University, New York, NY, in 2004 and 2006, respectively.

He was a Postdoctoral Research Associate with the MEMS Sensors and Actuators Laboratory, Department of Electrical and Computer Engineering, Institute for Systems Research, University of Maryland, College Park, from 2007 to 2008. He is currently a Postdoctoral Associate with the Department of Mechanical Engineering, Massachusetts Institute of Technology, Cambridge. His research interests are in the field of emerging power MEMS and microcooling technologies. His current efforts are focused on the development of ball-bearing-supported rotary micromachines, tribological characterization of microscale rolling contacts, nanostructured energy storage devices, sensors and actuators, and compact cooling systems.



Reza Ghodssi (S'92–M'96) is the Herbert Rabin Distinguished Associate Professor and Director of the MEMS Sensors and Actuators Laboratory, Department of Electrical and Computer Engineering, Institute for Systems Research, University of Maryland (UMD), College Park. He is also affiliated with the Fischell Department of Bioengineering, the Maryland NanoCenter, the University of Maryland Energy Research Center, and the Department of Materials Science and Engineering at UMD. He is the author or coauthor of more than 62 scholarly publications and the Coeditor of the *Handbook of MEMS Materials and Processes* (in press, 2009). He is an Associate Editor of *Biomedical Microdevices*. His research interests are in the design and development of microfabrication technologies and their applications to micro/nanodevices and systems for chemical and biological sensing, small-scale energy conversion, and harvesting.

Dr. Ghodssi is a member of the American Vacuum Society, the Materials Research Society, the American Society for Engineering Education, and the American Association for the Advancement of Science. He is the Cofounder of MEMS Alliance in the greater Washington area. He is an Associate Editor of the *Journal of Microelectromechanical Systems*. He was the recipient of the 2001 UMD George Corcoran Award, the 2002 National Science Foundation CAREER Award, and the 2003 UMD Outstanding Systems Engineering Faculty Award.

Dr. Ghodssi is a member of the American Vacuum Society, the Materials Research Society, the American Society for Engineering Education, and the American Association for the Advancement of Science. He is the Cofounder of MEMS Alliance in the greater Washington area. He is an Associate Editor of the *Journal of Microelectromechanical Systems*. He was the recipient of the 2001 UMD George Corcoran Award, the 2002 National Science Foundation CAREER Award, and the 2003 UMD Outstanding Systems Engineering Faculty Award.